Nuclear Materials and Energy 33 (2022) 101244

Contents lists available at ScienceDirect

Nuclear Materials and Energy

journal homepage: www.elsevier.com/locate/nme

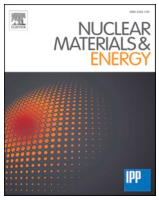

Influence of surface temperature, ion impact energy, and bulk tungsten content on the sputtering of steels: In situ observations from plasma exposure in PSI-2

M. Reinhart *, S. Möller, A. Kreter, M. Rasinski, B. Kuhn

Forschungszentrum Jülich GmbH, Institut für Energie- und Klimaforschung, 52425 Jülich, Germany

ARTICLE INFO

Keywords:
RAFM Steels
Tungsten surface enrichment
Surface morphology
Preferential sputtering

ABSTRACT

This study presents results from PSI-2 deuterium plasma exposures of reduced-activation ferritic martensitic steels with different tungsten content at a peak plasma flux of $9 \cdot 10^{20}$ D/m^{2}s and 420–920 K sample temperature. Via optical emission spectroscopy the relative sputtering yield of Fe and Cr, and via an infrared camera the evolution of surface morphology is studied in-situ in 2D. After the exposure, RBS, SEM and EDX reveal tungsten enrichment and the formation of surface structures. Due to the independent measurement of surface morphology and tungsten enrichment, it is possible to disentangle the impact of both effects on the erosion of Fe. As part of this study, we investigate the effects of tungsten content, sample temperature and ion impact energy. The results show a reduction of the sputtering yield, depending on the exposure conditions, up to a factor of 2 at 130 eV ion impact energy and 720 K sample temperature.

1. Introduction

Reduced activation steels such as Eurofer are envisaged as a structural material for future nuclear fusion power plants [1]. Using such steels also as plasma-facing material offers practical and economic benefits over tungsten (W), at least in areas of less than 2 MW/m^2 power loads [2]. The main drawback relates to the higher sputtering yields compared to W [3], limiting the lifetime and plasma performance. Recent result demonstrate that this disadvantage could be significantly smaller than sputtering theory suggests, due to the formation of surface nanostructures and an enrichment of heavy elements via preferential sputtering. Observations show the enrichment of W on the steel surface up to a few 10 % [4]. The thickness of these enriched layers is in the range of a few nm [5]. In addition, a surface morphology similar to W fuzz develops in a certain window of fluence and temperature [6]. Overall reductions of the sputtering yield by a factor of 10 can be observed [4], a quantity highly relevant for assessing where the steels could be employed in a fusion reactor.

The question arises which effect dominates the reduction of sputtering yield. Since the enriched layers are very thin [5], the quantification of the tungsten surface enrichment requires diagnostics with a high depth resolution. But even diagnostics like low energy ion scattering with a depth resolution of ~2 nm [7] do not show tungsten enrichment above 20 %. This suggests that the tungsten enrichment alone is insufficient for explaining a reduction of the sputtering yield by a factor of 10 [4], since this would require an enrichment > 90 %. Therefore, also the surface nanostructures must play an important role. The impact of nano-structuring on the sputtering yield was studied experimentally and theoretically. Latest SDTrimSP-3D calculations allow to investigate the mechanisms behind the suppression of sputtering. Reductions up to 75 % of the smooth surface sputter yields were calculated [8]. Also, experimental evidence for a strong impact of fuzz-like structures on the sputtering yield exist [9].

In the present study, our goal is to investigate the influence of the surface structures and the W surface enrichment at the same time. To separate both effects, we apply different types of diagnostics during the exposure (in-situ) and after the exposure (ex-situ). With Infrared (IR) camera imaging, we are able to follow the evolution of surface morphology in-situ [10]. At the same time, optical emission spectroscopy (OES) measures the emission from Fe and Cr lines in the plasma, which correlate to the erosion of Fe and Cr from the sample. With these two diagnostics, the erosion and the development of the surface morphology can be measured in-situ and time-resolved. This enables a deeper insight into the processes and enables faster parameter studies.

* Corresponding author.
E-mail address: m.reinhart@fz-juelich.de (M. Reinhart).

https://doi.org/10.1016/j.nme.2022.101244
Received 30 June 2022; Received in revised form 30 August 2022; Accepted 3 September 2022
Available online 9 September 2022

Additionally, the surface enrichment of tungsten is measured post-mortem by EDX and RBS, and the surface structures are investigated post-mortem with Scanning Electron Microscopy (SEM).

2. Experiments

Polished ($R_a \leq 20$ nm) $100 \times 80 \times 5$ mm^3 samples of the reduced-activation steels Eurofer (Eurofer 97 ~ 0.5 at.% W), Hiperfer (Hiper-Fer-Ta, ~2 at.% W + Ta) [11], and Crofer (fuel-cell steel Crofer 22H, ~1 at.% W) are prepared in the shape of the PSI-2 sample mask, see Fig. 1. The samples cover the whole sample holder, so no other material is exposed to the plasma beam, except for four M4 Mo-screws at the outer edges. No pre-outgassing or annealing is conducted.

For the plasma exposures, the hot-cathode linear arc-plasma device PSI-2 is used [12]. The PSI-2 base pressure is $8 \pm 3 * 10^{-8}$ mbar (dominated by H_2O) in all experiments. The impurity content leads to a few 10^{19}/m^2 O and C atoms on all samples after exposure, but their impact on the total erosion is neglected. The samples are exposed on the axial manipulator. Individual sample temperatures are recorded with the IR camera and a Type-K thermocouple on the sample backside. The sample holder also features a heating element, which is used to influence the sample temperature at constant plasma parameters. The plasma column has the typical hollow profile of PSI-2 [12], with the maximum plasma flux at a radius of 23 mm away from the plasma centre. In the centre of the plasma column, the plasma flux reaches only 25 % of the peak plasma flux. The selected plasma scenario with 50 A discharge current provides a peak flux density of $9.0 \pm 1.0 \cdot 10^{20}$ D/m^{2}s at an electron temperature of about 8 eV. The profile of the plasma flux along the plasma column radius is also shown as an overlay in Fig. 1. The plasma parameters were measured with a single tip Langmuir probe. A bias voltage can be applied to the sample holder, allowing to fix the ion impact energy at a constant value, and in a range between ~ 50–230 eV.

As mentioned in the introduction, the IR camera is used to measure the roughness of the sample in-situ during exposure. Most of the samples are prepared with 1 mm holes in the surface at 6 positions along the plasma radius (Fig. 1); only the Eurofer sample did not feature the holes in the sample surface, therefore IR emissivity measurements are not available for this sample. We assume that the IR emission from the holes is equivalent to black body emission with an emissivity of 1. These reference points can be used to calculate the emissivity of areas next to the hole, by comparing the ratios of the IR intensity measured by the IR camera as discussed in [10]. When the surface nanostructures are created and growing during plasma exposure, the measured emissivity increases due to a connection between surface coverage, thickness, and shape of the nanostructures to the IR emissivity. The IR emissivity has a limited probing range for nanostructures and saturates once the surface nano-structure thickness exceeds ~ 1 μm.

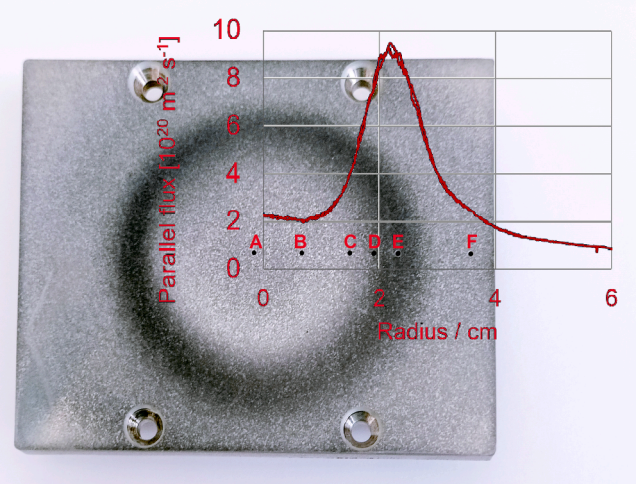

Fig. 1. Image of the Crofer sample exposed at 920 K. The darkening indicates the presence of surface nanostructures. The intensity of nano-structuring follows the plasma profile (overlayed graph of the plasma flux on the sample). Also visible are the holes prepared prior to the exposure for the IR Camera analysis labelled A - F.

The second in-situ diagnostic is the OES (2D Spectrometer). We use an Acton spectrograph with 0.75 m focal length and a resolution of 0.05 nm. Connected to the spectrograph is an Andor Solis EM-CCD Camera with a resolution of 1600x400 pixels. The view of the spectrometer is oriented perpendicular to the plasma column, and 5 mm in front of the sample. With this setup, we obtain a 2D image from each measurement of the spectrometer: Along the x-axis (1600 pixels) of the image, the spectrum is recorded with a bandwidth of around 25 nm. Along the y-axis, we acquire a spatial resolution of the full radial profile of the plasma column. However, the measured line intensities are integrated along the line-of-sight. To get an insight into the local intensities, especially in the centre of the plasma column, where the emission intensities are low, we apply a quick numerical Inverse Abel Transformation (Matrix Method) [13] with a high number of data points (equal to the number of pixels) to reduce the numerical error. During the plasma exposures, the spectrum is recorded between 408 and 433 nm, where a few bright iron and chromium lines (Fe I 423 nm, Ch I 425/427/429 nm) are visible, as well as the Balmer series line Dδ at 410 nm. The intensity of this Balmer line is used to correct for any changes in the transmission of the vacuum window. The transmission could reduce dynamically during the experiments due to coating of the windows with the eroded particles, therefore this effect needs to be considered. Reductions of the IR window transmission are not relevant, since the emissivities derive from a ratio of two IR measurement values, resulting in a cancellation of changes of the transmission.

In this study, 4 samples have been exposed to PSI-2. The detailed exposure conditions can be found in the first 4 rows of Table 1 and are not repeated here. After the plasma exposure, the surface structure is studied with Scanning Electron Microscope (SEM) (Zeiss Crossbeam 540) equipped with a focused ion beam (FIB) [14]. SEM images are taken of the surface, and the FIB cuts allow to estimate the depth of the nanostructures on the surface. In addition, tungsten enrichment on the surface is studied with energy dispersive X-ray spectroscopy (EDX) at an acceleration voltage of 3 kV. The low electron energy is selected to assure that the surface sensitivity is limited to a depth of about 50 nm. The surface composition is also analysed via 2.98 MeV ^{4}He ion-beam analysis in the Micro Nuclear Reaction Analysis (μNRA) station [15]. A 280 μm thick Si-detector with a resolution of 15 keV FWHM is used for Rutherford-backscattering spectrometry (RBS) and determination of the Particles*Sr value to an accuracy of ± 5 %. The analysis achieves a surface depth resolution of 21 nm. The spectra are analysed via SimNRA 7.03 [15].

3. Results

In the following paragraphs, the results of the Hiperfer samples (constant exposure at 920 K sample temperature and 230 eV incident ion energy) are exemplary shown in detail. Comparisons with the results of other sample types and exposure conditions are given at the end of this section.

In Fig. 2, the emission of the Fe I line at 423 nm is shown at the positions A to F over time for the Hiperfer sample. It must be noted that the measured intensities cannot be directly compared between the different measurement locations, because the plasma parameters are also varying. Since the intensity of the emission from the eroded iron in the plasma depends non-linearly on the plasma parameters such as electron temperature and density, a direct comparison of the intensities is not possible. Nonetheless, we can still compare the development of the intensities over time for the individual locations. Here we see that for all locations except A (center of the plasma) and F (outside the plasma), the

Table 1
Exposure conditions and key results of all experiments.

Sample type	Eurofer	Eurofer	Eurofer	Eurofer	Crofer	Crofer	Hiperfer
Experiment no.	1	1	1	1	2	3	4
Sample temperature	420	420	420	600	720	920	920
Ion impact energy	60	80	130	130	130	230	230
Relative erosion reduction (high flux)	0 %	0 %	7 %	13 %	50 %	20 %	31 %
Relative erosion reduction (low flux)	0 %	0 %	0 %	8 %	25 %	12 %	0 %
Erosion equilibrium fluence (high flux)	–	–	$7 \cdot 10^{23}$ D/m^2	$1.3 \cdot 10^{24}$ D/m^2	$8.6 \cdot 10^{24}$ D/m^2	$1.2 \cdot 10^{25}$ D/m^2	$1.0 \cdot 10^{25}$ D/m^2
Erosion equilibrium fluence (low flux)	–	–	–	$1.0 \cdot 10^{24}$ D/m^2	$6.5 \cdot 10^{25}$ D/m^2	$1.0 \cdot 10^{25}$ D/m^2	–
Surface structure equilibrium fluence (high flux)	–	–	–	–	$5.0 \cdot 10^{24}$ D/m^2	$4.7 \cdot 10^{24}$ D/m^2	$2.3 \cdot 10^{24}$ D/m^2
Surface structure equilibrium fluence (low flux)	–	–	–	–	$1.5 \cdot 10^{24}$ D/m^2	$1.8 \cdot 10^{24}$ D/m^2	$1.2 \cdot 10^{24}$ D/m^2
Tungsten surface concentration (high flux, RBS)	–	–	–	–	–	7 at.%	15 at.%
Tungsten surface concentration (low flux, RBS)	–	–	–	–	–	3 at.%	10 at.%
Tungsten surface concentration (high flux, EDX)	–	–	–	–	–	17 at.%	32 at.%
Tungsten surface concentration (low flux, EDX)	–	–	–	–	–	7 at.%	16 at.%

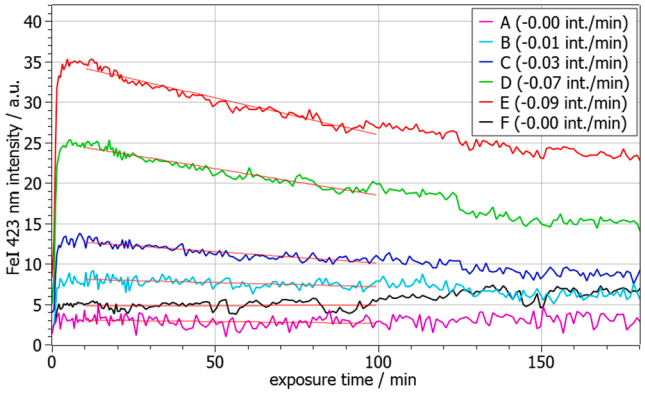

Fig. 2. Local intensity of the FeI 423 nm line emission 5 mm in front of the sample surface at positions A (center of the plasma column) to F (outside of the plasma column) over time for Hiperfer sample (experiment no. 4). Data are normalized to the Dδ line emission intensity. A linear fit is added with the slope indicated in the legend to identify if there is a decrease over time.

intensity is decreasing over time, which means that the erosion of Fe is reducing. In positions D and E with the highest plasma fluence, the Fe I line intensity reaches an equilibrium after ~ 180 min of exposure. This corresponds to a plasma fluence of $1 \cdot 10^{25}$ D/m^2.

Fig. 3 shows the results of the Cr I line at 425 nm for the same experiment. The same reduction over time as for the Fe I emission line can be observed, but the onset of the intensity reduction is delayed (after 20 min of exposure time compared to 5 min for Fe). Since the sputtering yields for D on Fe and on Cr are similar [16], we assume that the difference is related to the segregation of Cr to the surface caused by the high temperature of the sample [17]. Before the plasma exposure starts, the sample is pre-heated with the heating element of the PSI-2 sample manipulator. This could provide enough time at elevated temperatures for Cr to segregate to the surface. This Cr "reservoir" keeps the Cr erosion at a high level for the first 20 min of the exposure. After 20 min, the reservoir is depleted and the influence of the tungsten surface enrichment (reducing Cr erosion over time) is dominating. The linear fits added to the measurements show that there is a decrease over time for all measurement positions, also positions A and F, which do not show a decrease over time for the Fe I line (Fig. 2). From this we conclude that there is also a reduction of the Fe erosion in these locations, but the intensities of the Fe I line ion positions A and F are too weak to identify this with the current setup. There is also a shift of the intensities visible around minute 125, which is attributed to a small misalignment in the optical path.

Fig. 4 shows the emissivity of the Hiperfer sample surface during the same experiment. All points start at an emissivity of around 0.5 at the beginning of the plasma exposure. The increase of the emissivity during the plasma exposure is fastest in position E, the position where the highest plasma flux / fluence is present. Calculating the corresponding plasma fluence after which the emissivity reaches an equilibrium by considering the different plasma fluxes at each location shows that the saturation of the emissivity takes place at a fluence of $2.3 \pm 0.2 \cdot 10^{24}$ D/m^2 in positions E and $1.2 \pm 0.3 \cdot 10^{24}$ D/m^2 in position A. A saturation of the emissivity equals to the nano-structure thickness exceeding the sensitive range of the IR measurement. When the saturation is reached, small variations in the emissivity are noticeable when comparing the

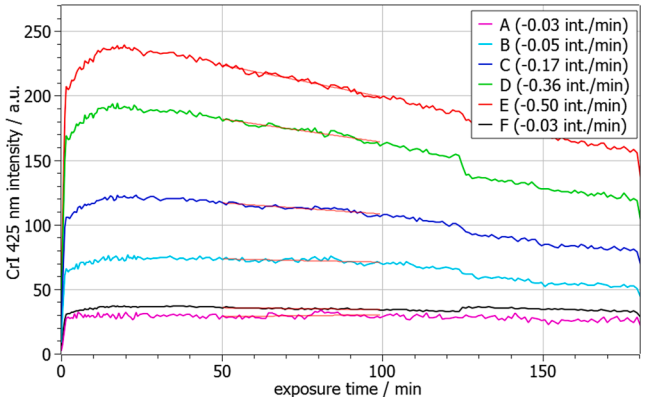

Fig. 3. Local intensity of the CrI 425 nm line emission 5 mm in front of the sample surface at positions A (center of the plasma column) to F (outside of the plasma column) over time for Hiperfer sample (experiment no. 4). Data are normalized to the Dδ line emission intensity. A linear fit is added with the slope indicated in the legend to identify if there is a decrease over time.

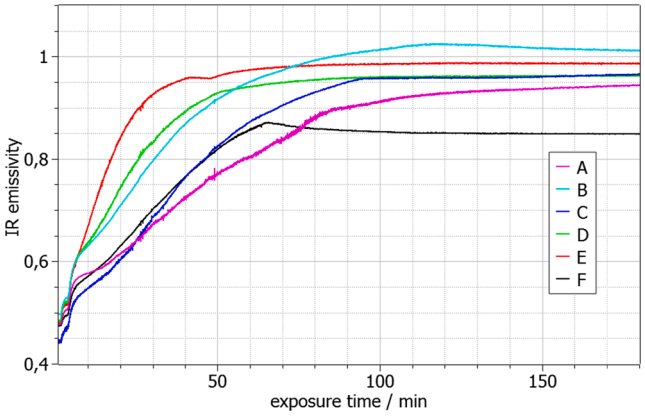

Fig. 4. Emissivity of the sample surface at positions A (center of the plasma column) to F (outside of the plasma column) over time for Hiperfer sample (experiment no. 4). The values feature a statistical uncertainty of 3% related to camera counting statistics and the uncertainty of the IR reference hole.

different locations, but most of them stay below the theoretical maximum of 1. The emissivity measured in position B exceeds the theoretical maximum, but this value is still within the measurement error. The saturation of the emissivity at 0.85 in position F could be caused by less pronounced surface nanostructures in this position. However, the SEM images (Fig. 5) show that the nanostructures in this position are comparable to the nanostructures in the other positions. Therefore, there is currently no explanation for this result. In the other experiments with the Crofer samples, the emissivity reached 1.0 also in position F.

There are also some intermediate variations in the slope visible in the emissivity time traces, despite constant exposure conditions. For example, for position E at t = 50 min, the emissivity increases again after it seemed to be saturated at t = 40 min. This could be caused by changes in the shape of the nanostructure. Temperature effects could also play a role, since a higher emissivity will affect the surface temperature, and the sample temperature is regulated only by measurement of the backside temperature sensor.

Comparing both in-situ measurements, we see that the erosion decreases with increasing surface roughness, but there is no direct relation between the measured reduction of the erosion via OES (which reaches an equilibrium only after a fluence of $1 \cdot 10^{25}$ D/m^2 in position E) and the measured surface nanostructure development (equilibrium at a fluence of $2.3 \pm 0.2 \cdot 10^{24}$ D/m^2 in position E). This indicates that the W surface enrichment plays an important role, and that it is still increasing after the surface nanostructures have reached an equilibrium. The RBS results after the exposure show a tungsten enrichment of up to 15 at.% in position E, decreasing in correlation with the plasma flux profile to 10 at.% in position A. At the same positions, the EDX results show an even higher tungsten enrichment of 32 at.% in position E and 16 at.% in position A. However, the EDX results might be influenced by the nanostructures on the sample surface. This could lead to an overestimation of the tungsten enrichment because electron reflection in the nanostructure causes additional excitation of X-rays [14]. For comparison, the tungsten surface enrichment of the Crofer sample exposed under the same conditions as the Hiperfer sample reaches only values of 7 at.% (pos. E) and 3 at.% (pos. A) (measured with RBS), or 17 at.% (pos. E) and 7 at.% (pos. A) (measured with EDX), respectively.

Figs. 5 and 6 show the results of the post-mortem SEM analysis. For the Hiperfer sample (Fig. 5), the nanostructures look similar in all positions, but the density and the depth of the structures are varying. As expected, we see the most dense and deep (around 1.5 μm) structures in position E at the peak plasma flux / fluence. This is confirmed by the appearance of the sample to the naked eye (Fig. 1) where a clear black ring can be seen only around position E. For comparison, SEM pictures from the Crofer sample at the same locations are shown (Fig. 6). This sample was exposed to the plasma under the same conditions as the Hiperfer sample. Again, the most pronounced surface structures can be observed in position E. But in general, the depth and density of the nanostructures on the Crofer sample are smaller than on the Hiperfer sample.

Finally, we summarize the results of all experiments in Table 1. The table shows the exposure parameters in the first 4 rows. The relative erosion reduction shows how much of a reduction in the Fe erosion is detected from the OES results. If no reduction is detected over time, the value is 0 %. The values are given for the high flux area (Position E) and the low flux area (position A) of the sample. For the same positions, also the fluence at which the measured erosion and IR emissivity does not change anymore ("Erosion equilibrium fluence" and "Surface structure equilibrium fluence"), and the tungsten surface concentration measured by RBS and EDX are shown in the last 8 rows.

For experiment no.1 with the Eurofer sample, no holes in the sample surface were prepared before the exposure. Therefore, there is no emissivity data available for the Eurofer sample. Also, the post-mortem diagnostic results are not available for the samples of experiments no. 1 and 2. Here, the sample temperature and ion impact energy were changed during the plasma exposure. This was done to investigate the influence of these parameters with the in-situ diagnostics during the experiment. But because of that, the influence of all different exposure conditions is "integrated" on the sample, and the post-mortem diagnostics would not give relevant results. The results for the different exposure conditions of experiment no.1 are also given in Table 1. For experiment no.2, only the first set of exposure conditions at 720 K sample temperature is given in the table, because the following exposure at 920 K sample temperature could not be completed. Instead, we repeated these conditions with experiment no.3 and a new Crofer sample. We can conclude from experiment no.1 that a minimum ion impact energy between 80 and 130 eV is required in order to detect a

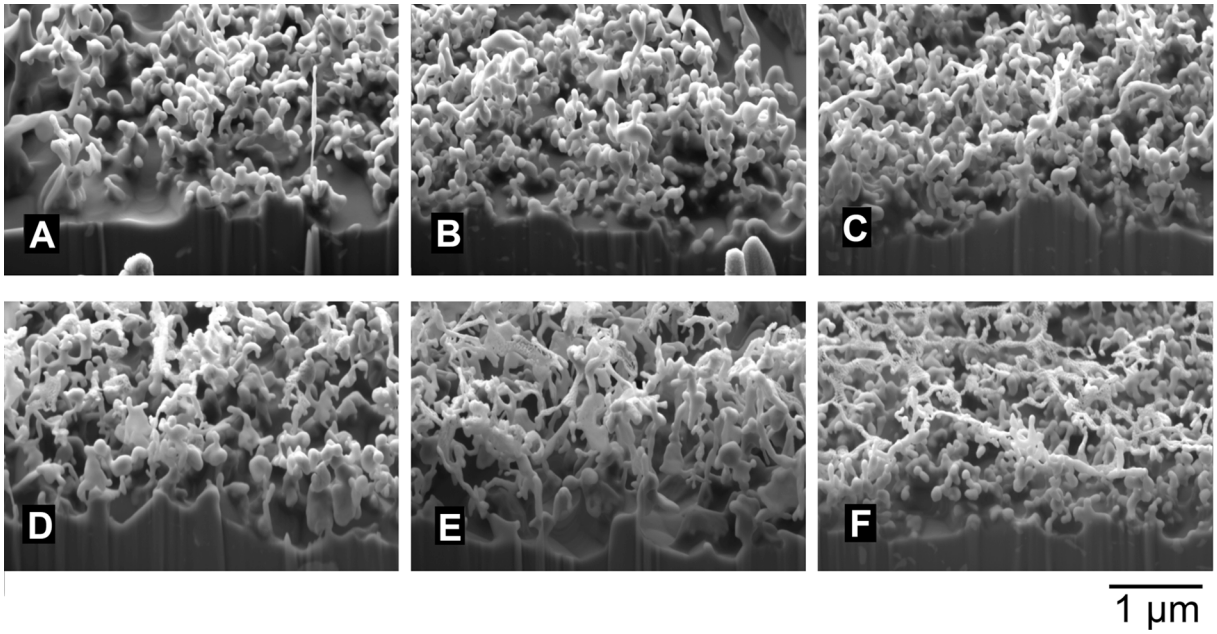

Fig. 5. Post-Mortem SEM images of Hiperfer sample (experiment no. 4) at positions A to F (with FIB cut in the bottom part of the single pictures for estimation of nanostructure depth). The figures demonstrate differences in height and density of the fuzz.

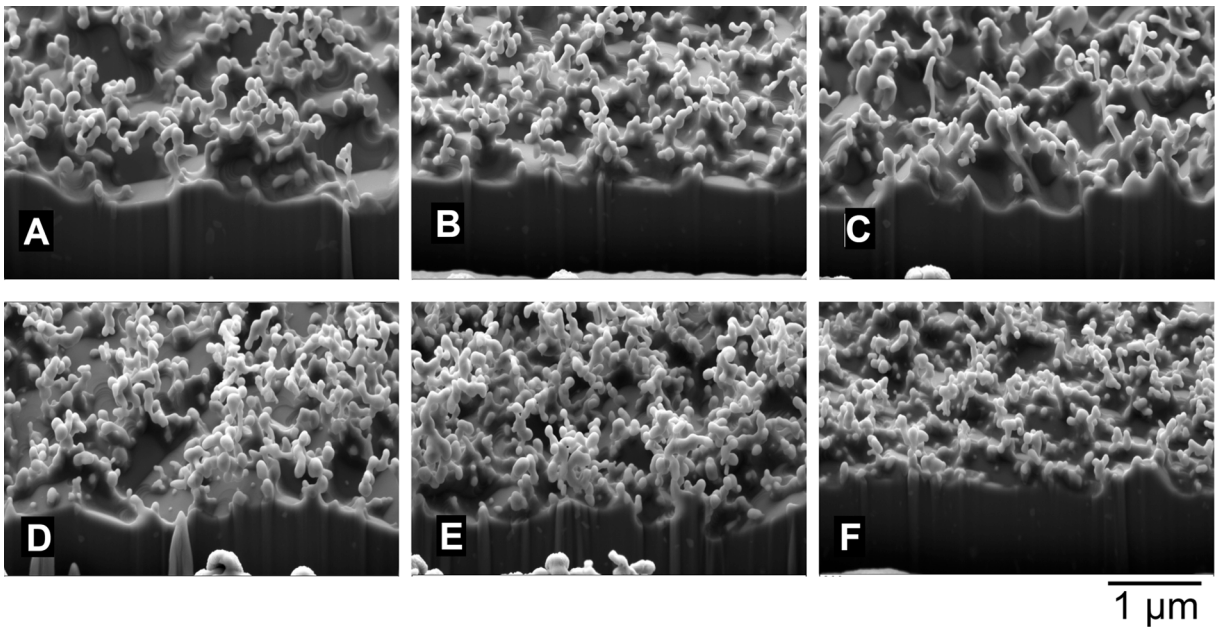

Fig. 6. Post-Mortem SEM images of Crofer sample (experiment no. 3) at positions A to F (with FIB cut in the bottom part of the single pictures for estimation of nanostructure depth). The figures demonstrate differences in height and density of the fuzz.

reduction of the Eurofer erosion. This minimum energy is directly related to the sputtering yields of D on Fe [16]. Below 80 eV, the ion impact energy is too low for significant erosion of Fe. The erosion reduction is also enhanced by the increase of the sample temperature from 420 K to 600 K. For the temperature range investigated with the two Crofer samples (720 K – 920 K) the opposite is observed: The erosion reduction effect reduces with an increase of the sample temperature from 720 K to 920 K. This suggests that there is an optimal temperature for the erosion reduction, likely between 600 K and 720 K. Regarding the tungsten surface enrichment, this optimal temperature range is also related to the balance of W surface segregation and diffusion. In previous studies, it was shown that there exists a temperature range with maximum tungsten segregation between 900 K and 1040 K for Eurofer [18]. At lower and higher temperatures, the segregation is suppressed by diffusion. The temperature range found in [18] is higher than the optimal temperature range found in the present work, but this can be explained by the additional influence of the surface nanostructures, and also by differences in the material composition between Eurofer, Crofer and Hiperfer.

The last experiment no. 4 with the Hiperfer sample and the same exposure conditions as in experiment no.3 also shows an enhancement of the erosion reduction effect with Hiperfer compared to Crofer. The lower fluence required for the surface structure to develop, and the higher tungsten enrichment in the surface, are backing this result. As previously mentioned, there is no reduction of the erosion in the area of lower flux (center of the plasma column) detected in experiment no.4 (Hiperfer). This is due to a low intensity of the measured Fe I line intensity in the center of the plasma column. The same is true for the first 3 cases of experiment no.1. But in the last case of experiment no.1, and in both experiments with Crofer, the intensity of the Fe I line is high enough to detect a reduction over time. This indicates (especially for experiment no.3 with the same exposure conditions as experiment no.4) that the absolute values of the erosion for Hiperfer are lower than for Crofer.

4. Conclusions

The 2D in-situ analysis of reduced-activation ferritic martensitic steels exposed to plasma in the linear plasma generator PSI-2 successfully demonstrated significant changes in the plasma response and sputtering rates of the investigated steels. The presented combination of OES, IR camera and post-mortem surface analysis represents a powerful method to investigate the impact of surface nanostructure evolution and W surface enrichment on the suppression of the erosion, and also the influence of various exposure parameters, most importantly sample temperature, ion impact energy and material composition.

With our first set of experiments, we can already demonstrate relevant relations between the different investigated parameters. The strongest suppression of the erosion by 50 % is found with Crofer at 720 K sample temperature. The suppression factors of > 100 seen in an earlier study [19] could not be confirmed here. As the sample temperature was increased to 920 K, we saw a reduction of the erosion suppression to only 20 %. At the same time, the in-situ observation of the surface structures did not reveal relevant differences between the 2 sample temperatures. From this, it can be concluded that a reduction of the tungsten enrichment in the surface, due to stronger W diffusion at higher temperatures [7], causes the reduction in the suppression of the Fe erosion. On the other hand, our experiments at lower temperatures show that the erosion suppression is increased if the sample temperature is increased from 420 K to 600 K. Therefore, an optimum for the sample temperature exists where the suppression of the erosion is at its maximum.

With the results from the Hiperfer sample, we can also conclude that the suppression factor increases with the initial tungsten content of the steel. The Hiperfer sample shows a suppression of the erosion during plasma exposure of 31 % (compared to 20 % for CroFer at the same exposure conditions). The results of the surface structure development and the tungsten surface enrichment also show an enhancement of these effects for Hiperfer compared to Crofer.

For the ion impact energies, our results from the Eurofer exposure show that there is a minimum energy between 80 and 130 eV, below that a suppression of the erosion is not detectable, related to the sputtering threshold of D on Fe.

In the future, additional parameter studies and post-mortem analyses need to be performed, to fill the gaps in our current set of experiments and give a clearer insight on the influence of the investigated parameters. Additionally, an accompanying study using sputtering models, which include surface nanostructure aspects and tungsten surface

enrichment, is ongoing to support the findings and the interpretation of our experiments.

CRediT authorship contribution statement

M. Reinhart: Conceptualization, Data curation, Formal analysis, Investigation, Methodology, Project administration, Resources, Software, Supervision, Validation, Visualization, Writing – original draft, Writing – review & editing. **S. Möller:** Conceptualization, Data curation, Formal analysis, Funding acquisition, Investigation, Methodology, Project administration, Resources, Software, Supervision, Validation, Visualization, Writing – original draft, Writing – review & editing. **A. Kreter:** Data curation, Investigation, Methodology, Project administration, Resources. **M. Rasinski:** Data curation, Investigation, Methodology. **B. Kuhn:** Data curation, Investigation.

Declaration of Competing Interest

The authors declare that they have no known competing financial interests or personal relationships that could have appeared to influence the work reported in this paper.

Data availability

Data will be made available on request.

Acknowledgments

The authors thank the PSI-2 Team, especially Michael Vogel and Sebastian Kraus for the reliable device operation.

This work has been carried out within the framework of the EUROfusion Consortium, funded by the European Union via the Euratom Research and Training Programme (Grant Agreement No 101052200 — EUROfusion). Views and opinions expressed are however those of the author(s) only and do not necessarily reflect those of the European Union or the European Commission. Neither the European Union nor the European Commission can be held responsible for them.

References

[1] K. Ehrlich, Materials research towards a fusion reactor, Fusion Eng. Des. 56-57 (2001) 71–82.
[2] H. Bolt, et al., Plasma facing and high heat flux materials – needs for ITER and beyond, J. Nucl. Mater. 307–311 (Part 1) (2002) 43–52.
[3] R. Behrisch, G. Federici, A. Kukushkin, D. Reiter, Material erosion at the vessel walls of future fusion devices, J. Nucl. Mater. 313-316 (2003) 388–392.
[4] K. Sugiyama, M. Balden, S. Elgeti, T. Höschen, M. Oberkofler, J. Roth, W. Jacob, Erosion of EUROFER steel by mass-selected deuterium ion bombardment, Nucl. Mater. Energy 16 (2018) 114–122.
[5] P. Ström et al., Sputtering of polished EUROFER97 steel: Surface structure modification and enrichment with tungsten and tantalum, J. Nucl. Mater. 508 (2018) 139–146.
[6] M. Balden, S. Elgeti, M. Zibrov, K. Bystrov, T.W. Morgan, Effect of the surface temperature on surface morphology, deuterium retention and erosion of EUROFER steel exposed to low-energy, high-flux deuterium plasma, Nucl. Mater. Energy 12 (2017) 289–296.
[7] H.R. Koslowski, et al., Temperature-dependent in-situ LEIS measurement of W surface enrichment by 250 eV D sputtering of EUROFER, Nucl. Mater. Energy 16 (2018) 181–190.
[8] U. von Toussaint, A. Mutzke, A. Manhard, Sputtering of rough surfaces: a 3D simulation study, Phys. Scr. T170 (2017) 014056, https://doi.org/10.1088/1402-4896/aa90be.
[9] R. Stadlmayr, P.S. Szabo, D. Mayer, C. Cupak, T. Dittmar, L. Bischoff, S. Möller, M. Rasiński, R.A. Wilhelm, W. Möller, F. Aumayr, Sputtering of nanostructured tungsten and comparison to modelling with TRI3DYN, J. Nucl. Mater. 532 (2020) 152019, https://doi.org/10.1016/j.jnucmat.2020.152019.
[10] S. Möller, O. Kachko, M. Rasinski, A. Kreter, C.h. Linsmeier, In situ investigation of helium fuzz growth on tungsten in relation to ion flux, fluence, surface temperature and ion energy using infrared imaging in PSI-2, Phys. Scr. T170 (2017) 014017, https://doi.org/10.1088/1402-4896/aa8a0a.
[11] S. Möller, B. Kuhn, R. Rayaprolu, S. Heuer, M. Rasinski, A. Kreter, HiperFer, a reduced activation ferritic steel tested for nuclear fusion applications, Nucl. Mater. Energy 17 (2018) 9–14.
[12] A. Kreter, C. Brandt, A. Huber, S. Kraus, S. MÖller, M. Reinhart, B. Schweer, G. Sergienko, B. Unterberg, Linear Plasma Device PSI-2 for Plasma-Material Interaction Studies, Fusion Sci. Technol. 68 (1) (2015) 8–14.
[13] W.R. Wing, R.V. Neidigh, A Rapid Abel Inversion, Am. J. Phys. 39 (7) (1971) 760–764.
[14] M. Rasinski et al., Performance of Eurofer97 under deuterium plasma exposure with seeded impurities at elevated temperature, Phys. Scr. T171 (2020) 014071 (5pp).
[15] S. Möller et al., A New High-Throughput Focused MeV Ion-Beam Analysis Setup, Instruments 5(1) Art. no. 1, (2021).
[16] Y. Yamamura, H. Tawara, Energy dependence of ion-induced sputtering yields from monatomic solids at normal incidence, At. Data Nucl. Data Tables 62 (2) (1996) 149–253.
[17] J. Shams-Latifi, P. Ström, E. Pitthan, D. Primetzhofer, An in-situ ToF-LEIS and AES study of near-surface modifications of the composition of EUROFER97 induced by thermal annealing, Nuc. Mater. Energy 30 (2022) 101139, https://doi.org/10.1016/j.nme.2022.101139.
[18] P. Ström, D. Primetzhofer, In-situ measurement of diffusion and surface segregation of W and Ta in bare and W-coated EUROFER97 during thermal annealing, Nucl. Mater. Energy 27 (2021) 100979, https://doi.org/10.1016/j.nme.2021.100979.
[19] T. Sarmah, P. Dihingia, M. Rahman, J. Ghosh, P. Chaudhuri, D.N. Srivastava, B. Satpati, S. Kumar, M. Kakati, G.D. Temmerman, Exposure of Indian RAFM under variation of He+ flux and target temperature in the CIMPLE-PSI linear device, Nucl. Fusion 60 (10) (2020) 106026, https://doi.org/10.1088/1741-4326/abae46.